J Paleolimnol
DOI 10.1007/s10933-008-9240-4

ORIGINAL PAPER

Recent occurrence of large jökulhlaups at Lake Tuborg, Ellesmere Island, Nunavut

Ted Lewis · Pierre Francus · Raymond S. Bradley

Received: 26 May 2008 / Accepted: 21 July 2008

Abstract The varved sediment record from glacially-fed Lake Tuborg, Ellesmere Island, Nunavut, shows that only three large jökulhlaups have occurred there in the last millennium: 2003, 1993, and 1960. Detailed analyses of sediment microstructure and particle size, combined with in-situ hydrometeorological and limnological process studies, allowed jökulhlaup facies identification and discrimination from deposits from other processes. Deposits from large jökulhlaups are anomalously thick, typically lack internal structure, have sharp bases, and fine upwards. The ice-dammed lake above Lake Tuborg (the source of the jökulhlaups) likely changed its drainage style in 1960, from ice-dam overtopping to ice-dam flotation and glacial tunnel enlargement by melt widening, which allowed the lake to drain completely and catastrophically. Complete drainage of ice-dammed lakes by ice-dam flotation is rare in the region is due to the pervasiveness of cold-based ice. Twentieth century warming is likely responsible for some combination of dam thinning, lake expansion and deepening, and changing the thermal regime at the base of the dam. Anomalously thick individual varves were periodically deposited beginning in the nineteenth century, and their thickness increased with time. This likely reflects a combination of increased ice dam overtopping, subaqueous slope failures, sediment availability and rising air temperature. The varve record presented here significantly correlates with a previous, shorter record from Lake Tuborg. However, generally weak correlations are found between the new varve time series, regional records of air temperature, and glacial melt from ice cores on the Agassiz Ice Cap. It is hypothesized that on short timescales, sedimentation at the coring location reflects a complex and varying integration of multiple hydroclimatic, geomorphic and limnologic influences.

Keywords Jökulhlaup · Varve · Ice-dammed lake · Canadian High Arctic · Lake processes

T. Lewis · R. S. Bradley
Department of Geosciences, Climate System Research Center, University of Massachusetts, Amherst, MA 01003, USA

T. Lewis (✉)
Department of Geography, Queen's University, Mackintosh-Corry Hall, Room D201, Kingston, ON, Canada K7L 3N6
e-mail: limno.ted@gmail.com

P. Francus
Centre Eau, Terre et Environnement, Institut National de la Recherche Scientifique, Quebec City, QC, Canada G1K 9A9

P. Francus
GEOTOP-UQAM-McGill, Montréal, QC, Canada H3C 3P8

Introduction

Most ice-dammed lakes studied in the Canadian High Arctic drain incompletely by overtopping their ice

dams (Maag 1969). However, in July 2003, a large ice-dammed lake on Ellesmere Island (Fig. 1b) drained subglacially by floating its ice dam. An englacial or subglacial conduit system developed, and the ice-dammed lake drained completely (Lewis et al. 2007).

The ice-dammed lake drained into Lake Tuborg (Fig. 1), a large lake with trapped sea water in one of its basins, and annual laminae (varves) in portions of its lake bottom (Smith et al. 2004). Monitoring of the 2003 *jökulhlaup* (Icelandic for glacier-burst), and examination of the resulting sedimentary deposits in Lake Tuborg, suggested that a characteristic thick, fining upward jökulhlaup-derived facies was deposited without eroding underlying sediments in a deep site far from the jökulhlaup inflow (Lewis et al. 2007).

Little was known about the frequency, magnitude, and drainage style of similar events in the past. This article presents an overlapping 515 cm sequence of varved sediment that was obtained from this deep, distal location, providing a unique opportunity to evaluate jökulhlaup activity for the last 1,060 years.

Few high-resolution reconstructions of jökulhlaup history have been attempted (Atwater 1984; Waitt 1984; Gilbert et al. 1997; Blais-Stevens et al. 2003), probably because of the potential for erosion of underlying sediments by hyperpycnal flows in proximal locations, and the potential for bypassing in distal locations, especially in the marine environment (Maria et al. 2000). At Lake Tuborg, a shallow sill protects distal locations from erosive hyperpycnal flows, as does an extremely dense and deep saltwater layer. The long, straight shape of the lake ensures that turbid jökulhlaup-generated overflow plumes are distributed through the lake, making sediment bypassing unlikely (Lewis et al. 2007; see Discussion).

This article builds upon previous varve studies at Lake Tuborg by using multi-annual lake and hydrometeorologic process studies to pinpoint an ideal coring location, and evaluate potential hydroclimatic forcings for sedimentary structures in the core record. In-situ process studies have been particularly informative, since Lake Tuborg has complex bathymetry, chemical and thermal stratification, and multiple sediment inputs. This work also triples the length of a previously published Lake Tuborg varve record (Smith et al. 2004). In addition, only two other glacially fed lakes in the Arctic have had the paleoenvironmental significance of their sediments studied (Lamoureux and Gilbert 2004; Chutko and Lamoureux 2008).

Site description and previous work

Lake Tuborg is located on north-central Ellesmere Island (Fig. 1a). Eureka is the closest Meteorological

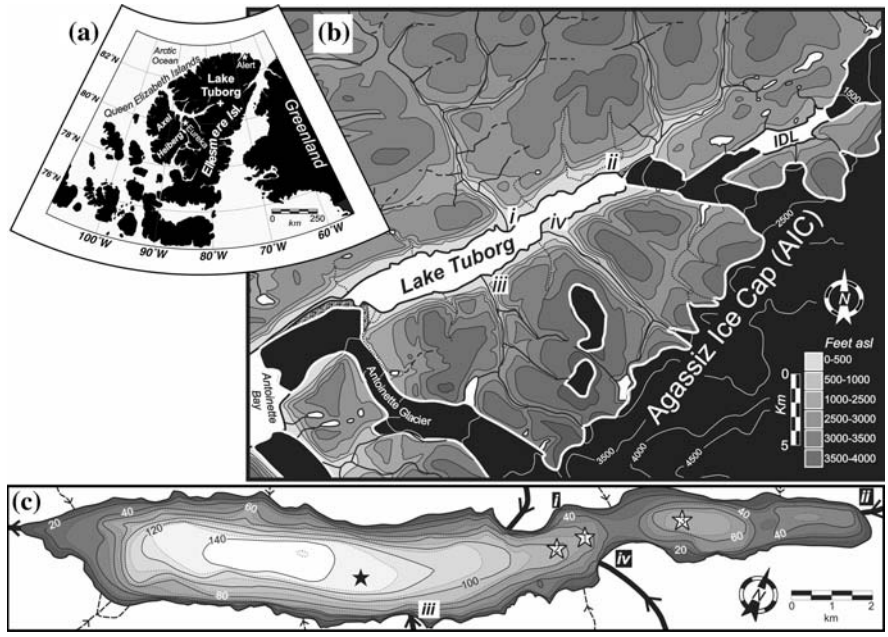

Fig. 1 (**a**) Location of Lake Tuborg on Ellesmere Island in the Canadian High Arctic. (**b**) Physiography and topography near Lake Tuborg and the ice-dammed lake (IDL). Contour interval is 500 feet; shading is feet asl. i through iv mark the mouths of the major rivers that feed Lake Tuborg. (**c**) Lake Tuborg bathymetry and coring locations. The black star is the location of the core sequence described here, and is at 80.95° N, 75.764° W. The white numbered stars are the locations of cores from Smith et al. (2004). Solid bathymetric contours are every 20 m

Service of Canada weather station (Fig. 1a; 220 km southwest; 10 m above sea level (ASL)), where mean annual air temperature from 1948–2003 was −20°C, and the only months with average temperatures above freezing were June (2.3°C), July (5.6°C), and August (3.1°C). On average, 32 mm of precipitation (snow and rain) fell at Eureka from June to August. The largest precipitation event lasted 4 days in mid-August, 1953, when 50.1 mm fell. On average, the largest June to August precipitation event is 10.8 mm ($\sigma = 7.8$ mm). Air temperatures at Lake Tuborg and Eureka are very similar, though it is typically, but not always, slightly warmer at Lake Tuborg (Table 1). In four summers of monitoring at Lake Tuborg, the lake generally received more precipitation than Eureka (Table 1).

Lake Tuborg is at 11 m ASL, and is separated from the sea at its outlet by sediments from a grounded arm of the Antoinette Glacier (Fig. 1b). Marine isolation occurred at approximately 3,000 years BP, based on ^{14}C measurements from bicarbonate in the trapped saltwater in the southwest basin (Long 1967). Watersheds surrounding Lake Tuborg are largely unvegetated and unmodified by humans, and are underlain by Lower Silurian to Lower Devonian Danish River Formation calcareous-dolomitic sandstone (Trettin 1996).

A large watershed feeding Lake Tuborg from the north is unglacierized at present, and sediment and water are transported during a brief period of peak nival melt in mid-to-late June (Fig. 1b, location i). After the supply of snow is exhausted in July, nival-fed streams largely dry up. However, two glacially-fed tributaries drain into Lake Tuborg at its south shore (Fig. 1b, locations iii and iv), and these are fed by the cold based Agassiz Ice Cap, which parallels the shoreline at 900 m ASL, and has an equilibrium line altitude of about 1,260 m ASL (Braun 1997). Hydrometeorologic monitoring at location iv showed that sediment transport responds in a complex, nonlinear way to weather and climate. As the freezing line moves up the ice cap during mid-to-late July, meltwater is temporarily stored in relatively small ephemeral supraglacial lakes. These lakes periodically drain into Lake Tuborg in discrete slush flow events, and transport large volumes of sediment over a period of days (Braun et al. 2000). Based on aerial photographs and field observations, this supraglacial meltwater ponding does not seem to occur in the watershed above location iii (Fig. 1b).

Table 1 Comparison of air temperature and precipitation at Eureka and Lake Tuborg[a]

	Temperature (°C)			Precipitation (mm)	
	Eureka	Lake Tuborg	*r*	Eureka	Lake Tuborg
1995	3.2	4.1	0.94	6.5	10.9
2001	4.2	3.8	0.90	31.2	97.1
2002	3.7	4.1	0.84	91.5	52.3
2003	4.7	5.1	0.92	23.4	27.7

[a] 1995 data (Braun et al. 2000) are for June only. 2001–2003 data are from May 28 to August 10. All records are from about 10 m ASL

An extremely large ice-dammed lake exists above the northeast corner of Lake Tuborg (Fig. 1b). The surface elevation of the full lake was 342 m ASL in February, 2003 (Zwally et al. 2003, updated 2007), and the lake dimensions are 6 × 1.5 km. The lake captures supraglacial meltwater from the Agassiz Ice Cap, and is normally completely isolated from Lake Tuborg. However, in 2003, the level of the lake rose enough to begin draining by overspilling its ice dam in early to mid July. Overspilling ended abruptly on July 25, when the lake catastrophically and entirely drained into Lake Tuborg. Between 3.2 and 5.5×10^8 m^3 of water drained, making the jökulhlaup the largest observed in Canada since 1947. It was triggered by ice-dam flotation, an extremely rare drainage style for Canadian High Arctic ice-dammed lakes. The 2003 event is described in detail in Lewis et al. (2007), and results pertinent to this study are summarized in the "Discussion" section.

Lake Tuborg has two basins separated by a shallow 34 m sill: a large 145 m deep saltwater basin to the southwest, and a smaller 74 m freshwater basin to the northeast (Fig. 1c). The saltwater basin has an extremely sharp and strong chemocline at 56 m depth that separates fresh water from dense underlying saltwater with a salinity of about 25 practical salinity units (PSU).

Lake level varies by about 1 m in typical summers. In 2003, lake level increased by 2 m while the ice-dammed lake was overspilling, and 8 m during the jökulhlaup.

Several factors promote undisturbed deposition of clastic varves in the saltwater basin. The severe climate only allows for river flow and sediment

transport during a brief period during summer (Braun et al. 2000), when relatively coarse particles are transported throughout the lake and deposited (Lewis et al. 2007). Over the long winter, clay-sized particles should slowly settle and form a clay cap on the summer deposits (Smith and Ashley 1985). The great depth of the basin (145 m), and the nearly perennial lake ice cover prevent wind-generated mixing of lake bottom deposits (Håkanson and Jansson 1983; Lewis et al. 2007). Physical mixing between the saltwater and freshwater layers is inhibited by the sharp and strong density difference, equivalent to 20,000 mg/l (Lewis et al. 2007). By contrast, hydrologic monitoring of the largest glacially-fed stream showed that hourly fluvial suspended sediment concentration was always less than 5.3 mg/l, even during slush flows (Braun 1997; Braun et al. 2000). Therefore, hyperpycnal flows should rarely—if ever—plunge below the chemocline and erode underlying sediments. Finally, anoxic conditions inhibit disturbance by bioturbation in the saltwater basin (Lewis et al. 2007).

Previous paleoenvironmental work on Lake Tuborg sediments was based on two percussion cores from the saltwater basin near the sill, and one from the freshwater basin (Fig. 1c; Smith et al. 2004). Sediments were interpreted as varves, and the available record was 300 years long. Distinctly thick often sand-rich deposits were interpreted as the result of high-magnitude catastrophic discharge events, and these events increased in frequency from the beginning of the nineteenth century until 1962. In addition, significant correlations were found between the varve thickness record and the record of melt layers on the Agassiz Ice Cap (Fisher et al. 1995), and 900 mB air temperatures at Eureka (Smith et al. 2004). However Smith et al. (2004) were unable to discriminate between slush flow deposits, jökulhlaup deposits, and other processes capable of producing thick coarse-grained deposits.

Methods

Sediment cores were obtained from Lake Tuborg in the central part of the saltwater basin, in 135 m of water (Fig. 1c). Three coring techniques were used to ensure continuous and undisturbed recovery of sediment. Two vibracores (475 and 387 cm) were obtained in 2001 using a Rossfelder VT-1 submersible vibracorer. Long cores were obtained with the vibracorer in extremely deep water without disturbing laminae through core barrel friction. An Ekman dredge was also used repeatedly before and after the 2003 jökulhlaup to obtain a continuous 22 cm stratigraphy of short cores (<13 cm each) of highly unconsolidated near-surface sediments (Lewis et al. 2007). Square polycarbonate tubing was used to carefully subsample dredged sediment, and sediment-filled tubes were shipped vertically. Finally, the coring location was revisited in June 2005, when an Aquatic Research percussion corer was used to obtain the uppermost 184 cm of sediment. This was needed because the jökulhlaup-derived deposit had not fully formed when the last Ekman core was obtained, due to a thick jökulhlaup-derived overflow plume over the coring location in August 2003 (Lewis et al. 2007). In addition, the upper 8–22 cm of the vibracores were disturbed during the coring process, and it was unclear whether the Ekman stratigraphy overlapped with the undisturbed section of the vibracores. The 2005 percussion core provided the necessary undisturbed overlap.

Cores were split lengthwise in the lab using a circular saw, Dremel tool, and carbide-tipped tile-scoring knife. Split halves were photographed at the Limnological Research Center LacCore facility at the University of Minnesota-Twin Cities. Digital linescan images were obtained with a Geotek Corescan-V at 20 pixels/mm resolution.

Undisturbed overlapping sediment slabs were removed from split core faces, epoxy impregnated, mounted on 7.6 × 2.5 cm glass slides, and ground to 30 μm thickness (Francus and Asikainen 2001). Impregnated and polished slabs were prepared from both vibracores, which allowed the identification of small-scale unconformities, and strengthened the varve-based chronology. An Epson V750-M Pro flatbed scanner was used at 2,400 dpi to image polished slabs and thin sections under plain and cross-polarized light using normally-oriented polarizing filters above and below the thin section (Lamoureux and Bollmann 2004). Discrete sand-rich layers, subannual laminae, and clay layers were counted, and their thicknesses were measured using the Export to Illustrator feature of Photoshop (Francus et al. 2002). Where laminae boundaries remained unclear, a Zeiss EVO scanning electron

microscope (SEM) was used in backscattered mode to obtain images of individual silt- and sand-sized particles under high magnification (Francus 1998).

Two varve counts were performed. The first was completed using only polished slabs; 831 varves were counted to a composite depth of 320 cm. Thin sections and SEM images were used in the second count, in addition to polished slabs; 990 varves were counted to the same depth. A much more accurate count was performed with the additional imagery, so only the second count is presented here.

Dry bulk density was measured every centimeter on Ekman cores and the percussion core, and every 5 cm on the vibracores using a 1 cm^3 constant volume subsampler (Håkanson and Jansson 1983). Dry bulk density between sampling points was modeled with a series of best-fit equations, and annual mass accumulation rate was calculated as the product of modeled dry bulk density and varve thickness (Schiefer 2006). Calculation of annual mass accumulation theoretically compensates for changes in dry bulk density near the sediment/water interface, compaction due to core barrel friction, and textural differences. However, changes in dry bulk density were relatively small in relation to changes in varve thickness, and the mass accumulation record is very similar to the unmodified varve record (Fig. 2).

To permit the use of parametric statistics, the annual mass accumulation time series was log-transformed to normally distribute the dataset, then standardized to a mean of zero and standard deviation of one (Ohlendorf et al. 1997; Rittenour et al. 2000). This process was also applied to the three varve thickness records in the Smith et al. (2004) dataset.

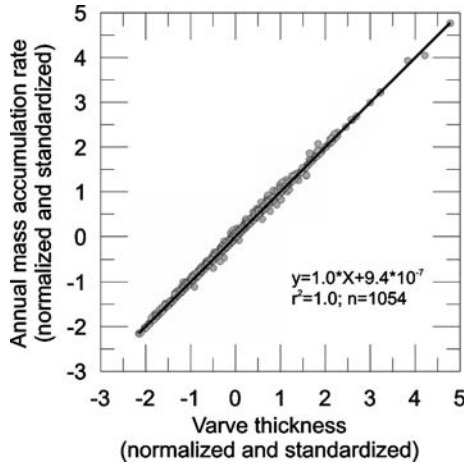

Fig. 2 Comparison of varve thickness with calculated annual mass accumulation rates. Varve thickness (originally in centimeters) and annual mass accumulation rate (originally in $g/cm^2/a$) time series have been log-normalized and standardized. Black line is the best-fit linear regression

Particle size was measured with a Coulter LS-200 laser diffraction particle-size analyzer. Subsamples were obtained every 0.5 cm in the core sequence, and were pretreated with hydrogen peroxide to remove organic particles, and a mixture of sodium hexametaphosphate and sodium carbonate to disperse aggregates (Head 1992). Slurries were shaken and sonicated before they were analyzed. Statistics were calculated by the moment method.

X-ray fluorescence (XRF) for determination of elemental composition was performed every millimeter on split cores on an ITRAX core scanner at the Institut National de la Recherche Scientifique. Exposure time was 10 s, voltage was 30 kV, and current was 30 mA.

X-ray diffraction (XRD) was performed for determination of mineralogy on seven samples using a Scintag XDS2000 in the Smith College Geology Department. Powdered samples were progressively scanned at 45 kV and 40 mA, from 2° to 62°, and the resulting diffraction patterns were compared with reference cards in the software DMSNT v.2.83.

Independent dating of sediment was attempted using ^{137}Cs, ^{210}Pb and ^{14}C. Alpha spectroscopy of ^{210}Pb, and gamma spectroscopy of ^{137}Cs and ^{226}Ra was performed on nine subsamples at the Environmental Radiochemistry Laboratory, University of Manitoba. Woody fragments were exceedingly rare in the highly-clastic, organic-poor sediment; however, one sample from near the base of the varve sequence (Fig. 3d) was dated at the National Ocean Sciences Accelerator Mass Spectrometry Laboratory (NOSAMS) in Woods Hole, Massachusetts (NOSAMS accession #OS-60427).

Results

Facies description

Depth in the sediment column is expressed as a composite of an overlapping stratigraphy of the vibracores, percussion core, and Ekman cores.

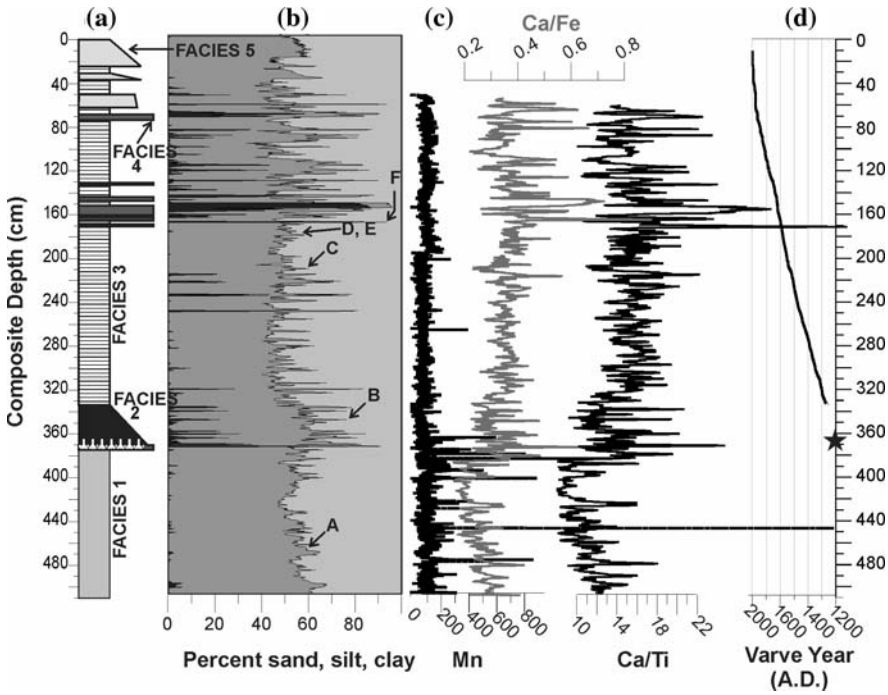

Fig. 3 (**a**) Core log, (**b**) grain-size, (**c**) XRF results, and (**d**) an age/depth plot. Symbols at the base of facies 2 in the core log represent sand, gravel, and woody fragments macrofossils. The grain-size plot shows percent sand (black), silt (dark grey), and clay (light grey), and the labels correspond to subpanels in Fig. 4. XRF units are peak area element integrals. XRF sample resolution is 1 mm; Mn data are not smoothed, Ca/Fe and Ca/Ti are 9-sample running averages. The star on the age/depth plot shows the location of the 84–389 A.D. 2σ calibrated radiocarbon date, which was significantly older than predicted by varve counts

Table 2 Mean grain-size statistics for facies 1 (largely structureless, basal muds), facies 2 (thick fining-upward microlaminated deposit with iron oxide bands and sands and wood fragments at its base), facies 3 (thin clay-capped laminae that typically fine upward), facies 4 (discrete sand beds), and facies 5 (fine-grained, largely massive deposits)

Facies	*n*	% of core sequence	Thickness (cm)	Thickness standard deviation	Grain size ($\overline{X}$; μm)	Sorting (σ)	$\sigma/\overline{X}$	Skewness	Kurtosis
1	1	24.5	n/a	n/a	10.2	10.9	1.08	1.74	3.60
2	1	6.5	n/a	n/a	17.4	19.4	1.11	1.54	2.14
3	1058	59.0	0.22	0.22	11.3	13.2	1.16	1.95	4.58
4	6	1.5	1.3	1.6	244.1	210.6	0.86	1.20	2.60
5	3	8.5	13.5	n/a	8.8	9.2	1.04	1.59	2.53

A composite core log is presented in Fig. 3a. Sediments are divided into five distinct facies based on grain size and internal structure (Fig. 3a; Table 2). Particle-size distributions for all facies except #4 have moderate peakedness, and are strongly skewed towards fine particle size. XRD results from each of the facies shows that all sediments are composed of quartz and calcite, with chlorite and muscovite also present; however, the proportions of each vary.

Facies 1, found in the lowermost 140 cm of the core sequence, is relatively structureless and low in sand content (Figs. 3a and 4a). It is geochemically unique compared to the rest of the cores sequence, as it contains high iron, titanium, and isolated manganese nodules (Fig. 3c). Facies 2 directly overlies facies 1, and is a 40-cm-thick, fining-upward sequence with diffuse orange laminae (Figs. 3a and 4b). Laminae containing matrix-supported gravel, sand, and woody fragments are particularly common near the base of facies 2. Facies 3 is a long sequence of thin laminae with light-coloured coarse bases that fine and darken upward to clay caps (Fig. 4c). On average, these are classified as fine to medium silt. Facies 4 are sand beds, and are defined as samples with more than half their particle size exceeding 62.5 μm (Fig. 4f). The sand beds interrupt facies 3, and consist of very coarse-grained, sandy deposits with sharp bases and tops, and very low coefficients

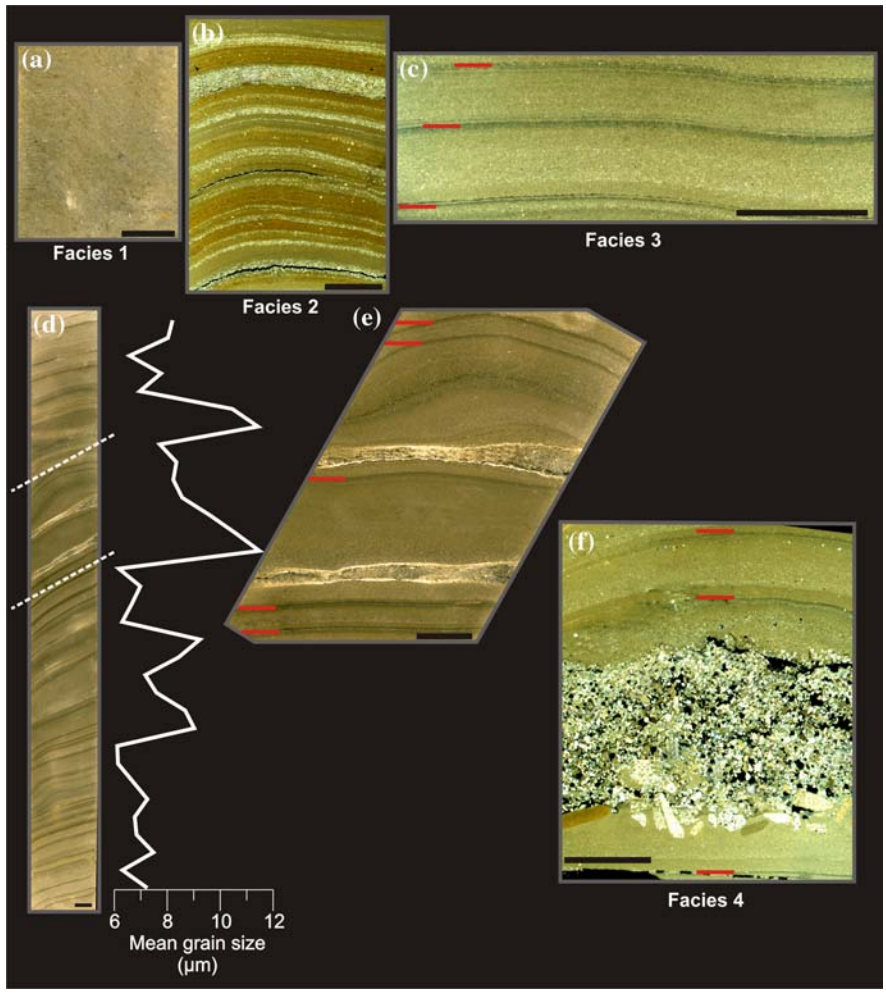

Fig. 4 Typical examples of facies 1–4. The location of each panel within the core sequence is shown on Fig. 3b. The black bar near the bottom of each image represents 0.5 cm. (**a**) Facies 1: massive sediments, (**b**) facies 2: a turbidite with iron oxide staining and microlaminated sands alternating with silty/sand layers, (**c**) facies 3; varves with dark clay caps (marked with red hashes), (**d**) a varve sequence presented with mean grain size, showing a fining-upward unit between the white dotted lines, (**e**) a close up of the area between the white dotted lines in (**d**), showing that two thin sand beds at the base of two varves were responsible for the fining-upward sequence, (**f**) facies 4: a sand-rich, grain-supported layer in the middle of a varve (clay caps are marked with red hashes). (**a**), (**d**), and (**e**) are flatbed scans of polished, epoxy impregnated slabs of sediment. (**b**), (**c**), and (**f**) are flatbed scans of thin sections under cross-polarized light

of variance (standard deviation, σ, divided by the mean, $\overline{X}$; Table 2). Facies 4 particle-size distributions are the least finely skewed, and are strongly peaked. Facies 5 also interrupts facies 3, but only three examples of these deposits were found, all within the upper 63 cm of the core sequence (Fig. 5). Two of these three deposits have sharp bases that fine upward (Fig. 5). Facies 5 is typically fine grained, although discrete, thin, coarse-grained beds are sometimes found within otherwise structureless sediment.

Dating

Peak ^{137}Cs activity occurs at 49.5 cm composite depth within facies 3 sediments (Figs. 5 and 6, sample 3). Clay layers were counted and measured, and compared with the depth of the ^{137}Cs maximum. If the clay layers represent winter deposition, the 1963 layer should correspond to the peak of atmospheric nuclear bomb testing in that year. The correspondence is well within the margin of error

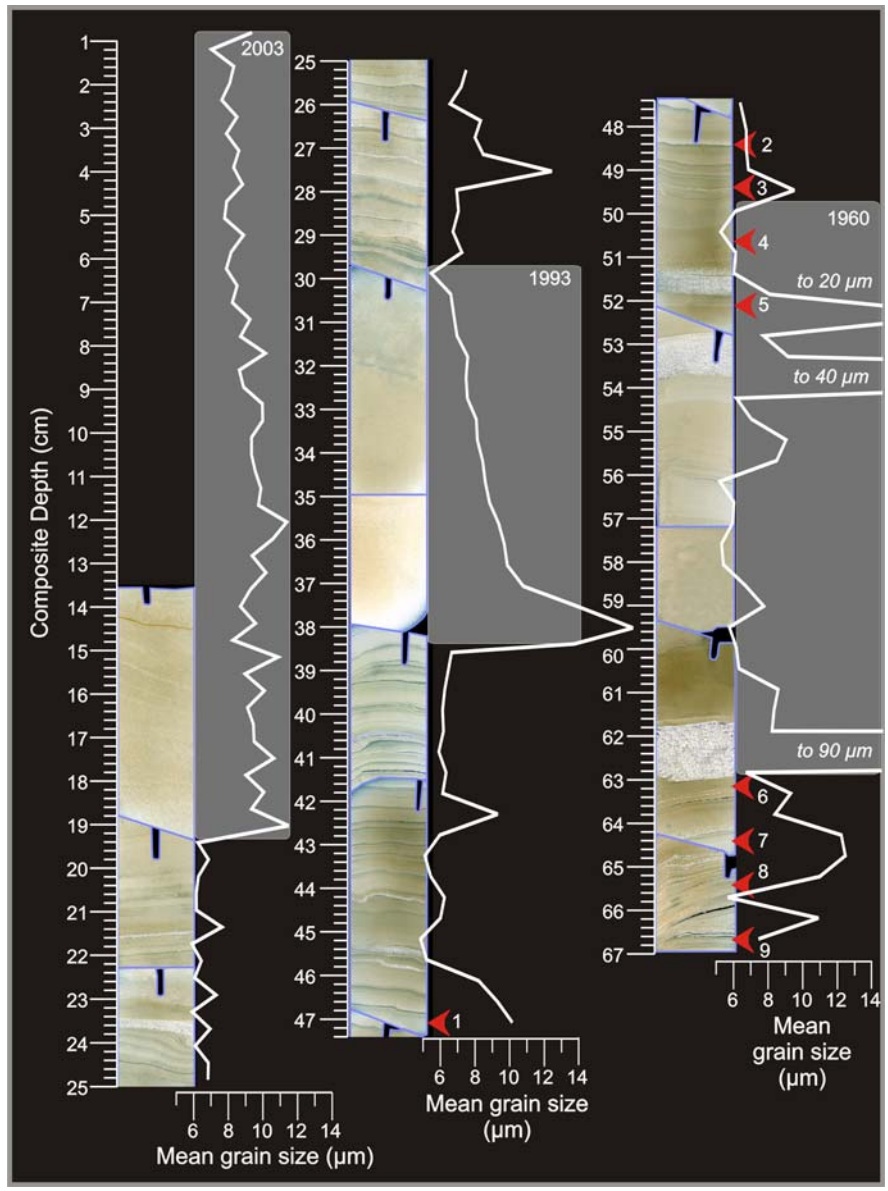

Fig. 5 Photomosaic of the upper 67 cm of the core sequence. Graphs show mean grain size. The 2003, 1993, and 1960 jökulhlaup deposits are highlighted in grey. The locations of ^{137}Cs and ^{210}Pb subsamples are the numbered red arrows, with the 1963 ^{137}Cs activity peak found at sample 3 (see Fig. 6). Images are flatbed scans of thin sections under cross-polarized light. Individual thin sections are outlined in blue, and notches at the top of sections are orientation marks. Cuts were made at an angle so the saw blade did not completely destroy any laminae. No thin sections are shown from the upper 13.5 cm of the sediment sequence because epoxy did not cure in clay-rich sediment that was saturated with saline water

from the thickness of the sediment slice (Fig. 6). In addition, the magnitude of the peak is consistent with peak ^{137}Cs activity previously measured in sediment from the saltwater basin of Lake Tuborg (Smith et al. 2004). Above the ^{137}Cs peak, activity is less than 2 Bq/g $\times$ 10^{-3} (Fig. 6, samples 1 and 2), which is consistent with the sharp decrease in atmospheric ^{137}Cs input after the Partial Test Ban Treaty was enacted (Wolfe et al. 2004). Directly below the ^{137}Cs activity peak is a 12.5-cm-thick facies 5 deposit (Figs. 5 and 6; see Discussion). Its position relative to the ^{137}Cs peak, and its lack of internal structure (except occasional sand beds) implies that it was deposited rapidly, and lamination counting suggests that this occurred around 1960. ^{137}Cs activity within this deposit is relatively high (Fig. 6, samples 4 and 5), which is consistent with deposition after bomb testing began, but before it was banned. ^{137}Cs activity was also measured in four samples below the thick massive deposit (between 63 and 67 composite depth; Fig. 5), and these had zero activity. This is consistent with sediment deposited before the late 1950s, which is supported by laminae counting, and the timing of the first appearance of ^{137}Cs in other arctic lakes

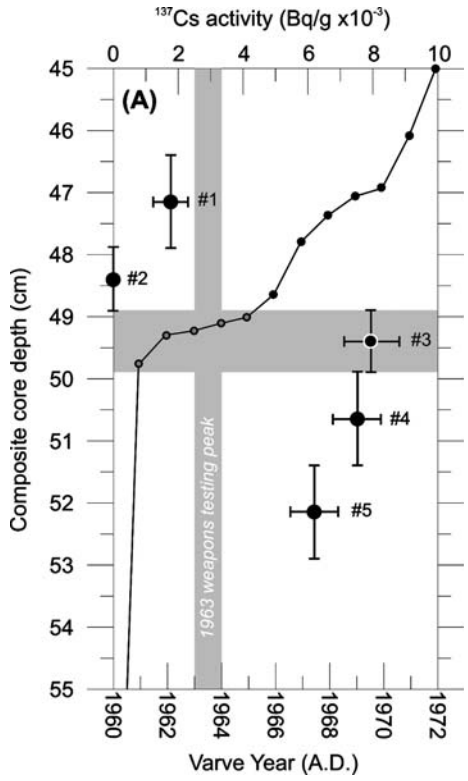

Fig. 6 Cesium-137 activity (symbols with error bars) and an age/depth plot (line) based on laminae counting. Below sample 3 is a 12.5 cm thick facies 5 deposit (Fig. 5). Horizontal error bars are 2σ, vertical bars represent the thickness of the subsampled slice. Four additional samples below sample 5 have zero activity between 63 and 67 cm composite depth (Fig. 5)

(ex. Stewart et al. 2007). Based on these results, and the classic varve-like structure of the sediments described here (Fig. 4c), we conclude that facies 3 are varves.

Results from analyses of ^{210}Pb and ^{226}Ra show that ^{210}Pb cannot be used as a dating tool, both for the sediment sequence discussed here, and for previously studied sediments from the saltwater basin of Lake Tuborg (Smith et al. 2004). There is no consistent downcore trend in ^{210}Pb activity both with respect to depth and age. Furthermore, ^{226}Ra activity frequently exceeds ^{210}Pb activity, making it impossible to separate ^{210}Pb produced in-situ from atmospherically derived ^{210}Pb. However, excess ^{210}Pb was found at 65.5 cm composite depth, which implies that sediments at this depth are younger than 150 years old (Wolfe et al. 2004). Lamina counting suggests that sediment at this depth was deposited around the mid twentieth century.

A woody fragment from 365 cm depth (Fig. 3d) yielded a ^{14}C age of 1790 BP $\pm$ 65 (2σ calibrated age = 84–389 cal AD; Stuiver and Reimer 2005). The woody fragment was found in facies 2 sediment, but if the mean annual sedimentation rate was the same as for facies 3, the woody fragment is 360 years older than expected (Fig. 3d).

Identification and occurrence of facies 5 deposits

Deposition at the coring location during the 2003 jökulhlaup was described in Lewis et al. (2007) as a 6-cm nearly massive deposit with a sharp, relatively coarse-grained base that fined upward. However, a thick overflow plume was present at the time of coring in August, 2003 so the deposit had not yet fully formed. The percussion core subsequently obtained in 2005 also clearly shows the fining upward sequence, but the jökulhlaup deposit had thickened to 19.5 cm (Fig. 5). Unfortunately, epoxy impregnation of the saltwater-saturated, very fine-grained, near-surface sediments in the percussion core was not successful, and thin sections from this zone could not be made. Nevertheless, incompletely cured slabs and core photographs revealed no laminations.

Facies 5 sediments are identified based on their nearly massive texture and anomalous thickness. Only three similar instances are found in the entire 1,060 year core record: in 2003, 1993, and 1960. The 2003 and 1993 deposits also have sharp bases that fine upward. The 1960 deposit contains three discrete centimeter-scale sand-rich beds, which fine and thin upward (Fig. 5; see Discussion).

The 2003 jökulhlaup deposit is extremely thick compared to all other laminae in the 1,060 year record, and compared to the other two facies 5 deposits. It is 4.8 standard deviations greater than the mass accumulation time series mean (Fig. 7a, c). The three facies 5 deposits are a major source of the pronounced rise in interannual variance in the late twentieth century, which has been more subtly increasing since about 1700 (Fig. 7e, f).

Comparisons with the Smith et al. (2004) time series and the Eureka climate record

The new Lake Tuborg varve records significantly correlate with the 300-year Smith et al. (2004) time series. The highest correlations generally occur with

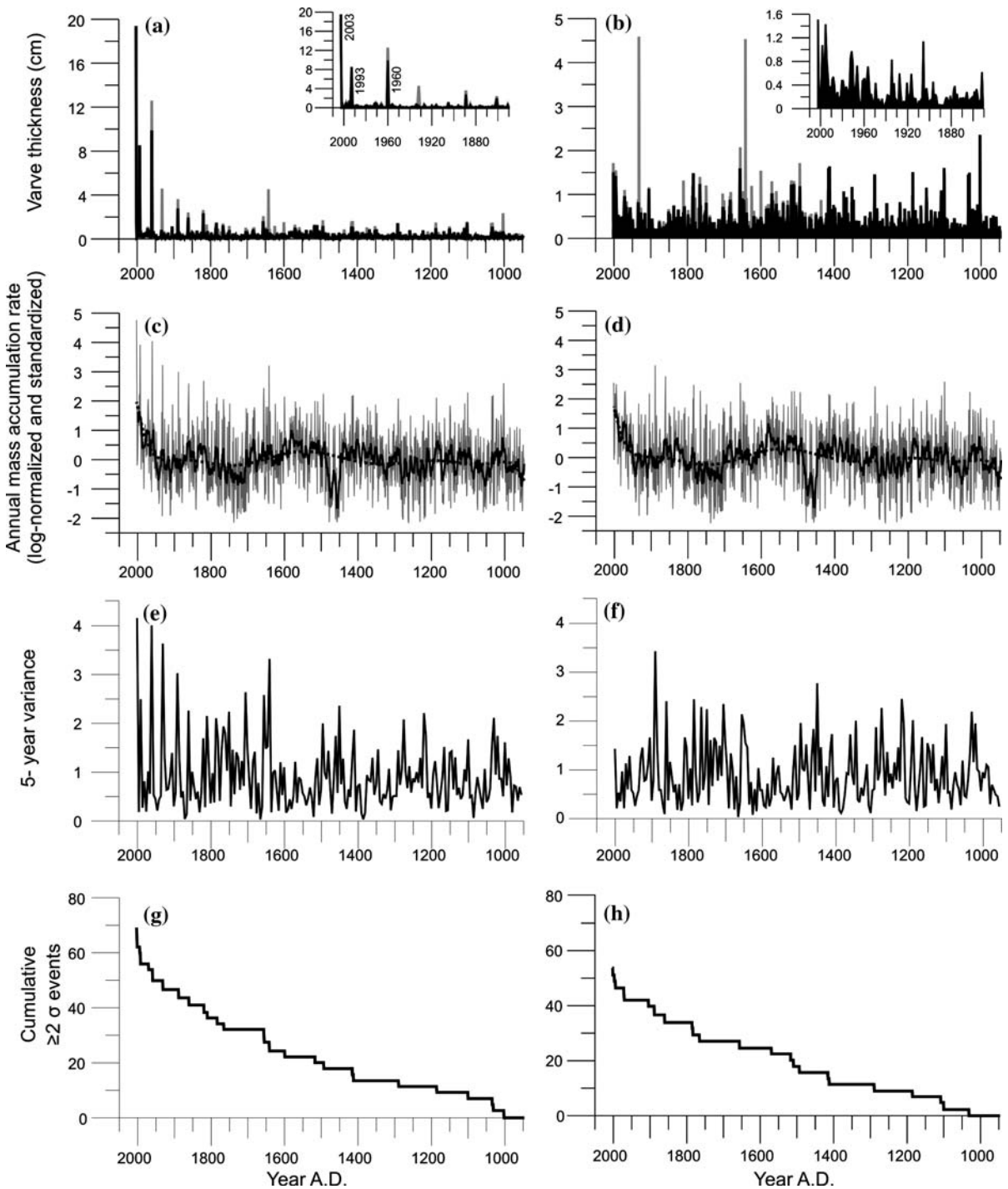

Fig. 7 Lake Tuborg varve thickness and annual mass accumulation rate. Panels on the left are time series that include jökulhlaup deposits, and panels on the right are with jökulhlaup deposits removed. Inset graphs on the topmost series show varve thicknesses since 1850. Grey plots in (**a**) and (**b**) represent the contribution from sand layers within each varve. Panels (**c**) and (**d**) show mass accumulation rate; the grey line is a plot with annual resolution, the black line is a nine-year running average, and the dashed line is a polynomial best-fit curve. Panels (**e**) and (**f**) show interannual variance with a 5-year window. Panels (**g**) and (**h**) are the cumulative sums of annual accumulation rates $\geq 2\sigma$ above the mean

Table 3 Correlation coefficients (r) comparing the Lewis et al. (2007) time series with the Smith et al. (2004) record

			Smith et al. (2004)			
			All Cores		Saltwater basin cores only	
			5-year	9-year	5-year	9-year
Lewis et al. (2007)	Unadjusted	5-year	0.21		0.3	
		9-year		0.47		0.44
	No jökulhlaups	5-year	0.18		0.25	
		9-year		0.42		0.39
	No jökulhlaups, no coarse deposits	5-year	0.22		0.26	
		9-year		0.42		0.39

Notes: The Lewis et al. (2007) time series is presented in an unmodified form, with jökulhlaup deposits removed, and with coarse-grained deposits removed. The Smith et al. (2004) time series is presented using all three of their cores, and only the two that were obtained in the saltwater basin. Annual data were smoothed using 5- and 9-year running averages. All correlation coefficients are significant at $p < 0.05$

9-year averages that are not adjusted by removing coarse-grained deposits and jökulhlaup deposits (Table 3).

Smith et al. (2004) noted significant correlations between their varve series and the melt record on the Agassiz Ice Cap ($r = 0.58$, $p < 0.01$). The new varve series is poorly correlated with the Agassiz melt record ($r = 0.19$, $p = 0.308$ for the last 300 years, and $r = 0.03$, $p = 0.661$ for the entire record). It is also poorly correlated with air-temperature records from Eureka, both at the surface and aloft. For example, 1,260 m is roughly the equilibrium line altitude of the Agassiz Ice Cap near Lake Tuborg, and interpolated temperatures at this elevation are poorly correlated to the new varve record ($r = 0.08$, $p = 0.308$; see Discussion).

Discussion

We hypothesize that large catastrophic jökulhlaups triggered by ice-dam flotation drained via subglacial and englacial conduits, that they produced facies 5 sediments, and that they began only in 1960. To support this argument, we will review the monitoring of the processes and deposits of the 2003 jökulhlaup (Lewis et al. 2007). Next, we will demonstrate that large jökulhlaup deposits (facies 5) are unique compared with all other sediments. The likelihood of either not recognizing a jökulhlaup deposit, or of incorrectly attributing a facies 5 deposit to another process will be assessed. We will compare the varve record to records of glacial activity in the region and the results from Smith et al. (2004). Lastly, we will argue that the chronology presented here is sufficiently robust to support our conclusions.

The 2003 jökulhlaup

Discharge from the jökulhlaup entered the freshwater basin at its northeast end via a subglacial portal (A; letters are labeled on Fig. 8). This basin completely filled with extremely turbid, cold, low-conductivity water derived from the ice-dammed lake. Evidence of lake bottom erosion and hyperpycnal flows was found here (B). Hyperpycnal flows in the saltwater basin were limited to areas close to the sill (C) for several reasons. First, the sill effectively blocked the strongest and most erosive bottom flows. Also, in the saltwater basin, the abrupt and strong density difference between the underlying saltwater layer and the overlying freshwater ensured that the two water bodies remained largely isolated. Small Kelvin–Helmholtz billows formed as extremely cold, sediment-laden water from the ice-dammed lake flowed just above the chemocline (D). This allowed sediment-laden interflows to mix with saltwater, flocculate, and quickly deposit their sediment close to the sill (E). Finally, the long distance (15 km) between jökulhlaup inflow and the saltwater basin coring location (F), and the shallow slope between the sill and coring location (1° average) also ensured that gravity-driven currents did not reach the coring site. Sediments at the coring site were largely delivered by a thick and extensive overflow plume (G). This produced a thick, largely massive deposit with a sharp base that fined upward, which was distinct from the laminated sediments underlying the jökulhlaup deposit (F; Lewis et al. 2007).

The unique character of large jökulhlaup deposits

Facies 1 is largely structureless (Fig. 4a), and could be described as fining upward, and in this sense facies 1 is

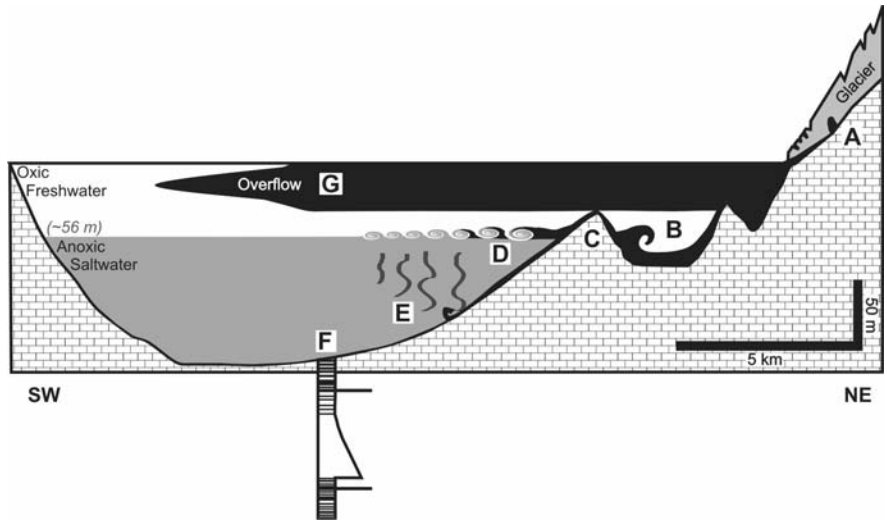

Fig. 8 Diagram of the 2003 jökulhlaup and the resulting lacustrine processes and deposits produced in Lake Tuborg (summarized from Lewis et al. 2007). Jökulhlaup inflow arrived from a portal at the northeast end of the northeast basin. The large saltwater basin is to the left of the figure, and the saltwater layer is shaded. The log is a representation of the 2003 jökulhlaup deposit overlain and underlain by thin varves and sandy layers. Labels A-G are explained in the Discussion section. Drawn to scale with a 100× vertical exaggeration

similar to large jökulhlaup deposits (facies 5; Fig. 3b). However, facies 1 is geochemically unique from all overlying sediments, as shown by the XRF data in Fig. 3c. While we remain unsure of the process that deposited facies 1, these sediments clearly have different provenance than overlying sediments, and were likely deposited under oxic conditions.

Facies 2 is thick and fines upward (Fig. 3a, b). However, unlike facies 5, terrestrial macrofossils, sand, and gravel are found at its base, and iron-stained silt and clay layers alternate with sandy laminae. This strongly suggests that the source of this deposit is the rivers or slopes surrounding the saltwater basin. It is unlikely that sand, gravel, and woody fragments were transported from the northeast basin. The fining-upward character, orange staining, and coarse laminae suggest deposition from a pulsating underflow that delivered oxidized water to the lake bottom (Weirich 1986; Scranton et al. 2001; Best et al. 2005).

Sands might be transported into the saltwater basin during jökulhlaups either directly in strong hyperpycnal flows that manage to overtop the sill, or indirectly from subaqueous slope failures triggered by rapidly rising and falling lake levels or oversteepening of the sill. These are likely sources of the three relatively thin sand beds in the 1960 facies 5 deposit (Fig. 5). By contrast, the sand-rich facies 4 sediments are much coarser grained, and the tops and bottoms of these deposits are sharp; resumption of varve-like rhythmic laminations is immediate (Fig. 4f). It is therefore unlikely that facies 4 sediments were deposited by large jökulhlaups, since a strong overflow would be produced, and a thick fining-upward sequence would be deposited on top of the sand beds (Fig. 8). Rather, facies 4 sand beds could have been deposited by subaqueous slope failures and melt-out of niveo-aeolian material deposited on the lake ice (Lewis et al. 2002). Hyperpycnal flows are less likely given the chemical stratification of the saltwater basin, but could potentially be generated by extremely turbid runoff associated with rare but intense precipitation events (Gilbert et al. 2006), slush-flows (Braun et al. 2000), exceptional glacial melt, and peak nival melt. All of these processes would necessarily have their sources in the saltwater basin and the tributaries and watersheds that drain into it.

Finally, it is unlikely that an overflow plume derived from a large jökulhlaup could bypass the coring location, given the long, straight shape of Lake Tuborg, and the extensiveness of the 2003 plume.

Other potential origins for facies 5 deposits

If a process other than a jökulhlaup could deposit units with all the characteristics of facies 5, then it has not happened more than twice (1993 and 1960). Slush flows (Braun et al. 2000) are an unlikely source of the deposits, based on results from monitoring and core lamination thicknesses. The 1995 varve, which was presumably influenced by the 1995 slush-flow events (Braun et al. 2000), has the 14th highest annual mass accumulation of the 1,060 year time series (it is 1.5 cm thick, and is 2.4σ above the time series mean). However, it is 80% thinner (7 cm thinner or 11 g/cm^2 less mass accumulation) than the thinnest facies 5 deposit. It is therefore clearly distinguishable from the deposits identified as large jökulhlaups. Maximum discharge and volume of the 1995 slush-flow events was several orders of magnitude less than the 2003 jökulhlaup. Slush flows also occurred in 2003 prior to the jökulhlaup that year. CTD casts showed that lacustrine sediment plumes from these events were strongly attenuated with distance. As a consequence, the 2003 slush-flow deposit at the coring location was less than 1.5 cm thick (Lewis et al. 2007).

Another process capable of producing anomalously thick deposits is intense rainfall (Lamoureux et al. 2001; Gilbert et al. 2006). In 2001, June to August rainfall at Lake Tuborg was extremely high, both compared to previous seasons of in-situ monitoring, and compared to the long-term precipitation record from Eureka (Table 1). From early June until August 10, 97 mm of rain fell at Lake Tuborg, which slightly exceeds the wettest summer in the 56 year Eureka precipitation record (2002; Table 1). Interestingly, only 50 mm of precipitation fell over the same period at Eureka in 2001. One eight-day period of continuous rainfall at Lake Tuborg produced 47 mm of precipitation in late July 2001; rainfall on two of these days was quite intense, totaling 18 and 15 mm. Discharge and sediment flux at the major deltas increased greatly. However, the coring location was not sensitive to this extreme precipitation; the 2001 varve is in the 43rd percentile for mass accumulation.

Finally, the massive structure of facies 5 sediments are unlikely to have been caused by bioturbation given that the saltwater layer is anoxic. Dissolved oxygen below the 56 m chemocline was <1 mg/l in 2003 (Lewis et al. 2007).

Ice-dammed lake drainage style, volume, and jökulhlaup magnitude

The 1960 deposit is anomalously thick compared to any annual layer before it. Its abrupt occurrence strongly suggests that the ice-dammed lake began draining completely by ice-dam flotation and tunnel development at this point. Prior to 1960, the ice-dammed lake likely drained incompletely by overtopping its dam. The ice-dammed lake drained this way for several weeks in July 2003, before a glacial conduit system developed, allowing catastrophic and complete drainage. The most common style of drainage in the region is ice-dam overtopping, at least prior to 1963 (Maag 1969).

An abrupt change in drainage style and/or jökulhlaup volume is also consistent with the anomalous microstructure of the 1960 deposit compared to the facies 5 deposits from 1993 and 2003. The 1960 deposit contains three centimeter-scale well sorted sand beds with discrete tops and bottoms, and the thickness and grain size of these beds decreases upwards (Fig. 5). Observations made during the 2003 jökulhlaup help explain these discrete sand beds. The ice-dammed lake drained extremely quickly, raising and lowering the level of Lake Tuborg by 8 m in 8 days (Lewis et al. 2007). Such rapid changes in lake level might cause extensive subaqueous slope failures. During the first large jökulhlaup in the history of the lake, nearshore sediments would be particularly prone to mobilization, since they would have been accumulating on the nearshore subaqueous and subareal slopes for at least a millennium under presumably much more stable lake-level conditions.

The thickness (and mass accumulation) of a jökulhlaup deposit is likely related in a complex way to the volume of water drained, hydrograph shape (Rushmer et al. 2002; Old et al. 2005), sediment availability, and the proportion of sediments transported by hyperpycnal versus hypopycnal flows. This, and the small number of deposits, makes it very difficult to attribute causes for the observed differences in facies 5 thickness.

The varve record and local and regional records of glacier activity and climate

It is hypothesized that warm air temperatures in the twentieth century caused the depth of the

ice-dammed lake to increase, or its dam to thin, which allowed the lake to drain by ice-dam flotation beginning in 1960. This is consistent with the progressive but episodic increase in varve thickness (and annual mass accumulation) after 1900 A.D. (Fig. 7d). It is also consistent with records of glacier activity in the region that show widespread recent negative mass balance, glacier retreat, and calving. Ice cores from the Agassiz Ice Cap, taken 55 km southeast of Lake Tuborg, show that twentieth century melt is unprecedented in the last 3,000 years (Fisher et al. 1995). This record does not continue after 1960; however, the Drambuie Glacier, an outlet glacier on the northeast side of the Agassiz Ice Cap, 110 km southeast of Lake Tuborg, has experienced almost wholly negative melt-driven mass balance since 1977, and the rate of loss is increasing (Koerner 2005). Shorter term, but more widespread, laser altimetry measurements on Ellesmere Island show extensive and rapid ice-cap thinning, mostly at lower elevations near their margins, below 1,600 m ASL. For example, between 1995 and 2000, ice elevations were reduced by >40 mm/year at the head of Otto fiord, 140 km west-northwest of Lake Tuborg. The thinning occurred when air temperatures at Eureka were 0.7°C warmer than the record as a whole, and occurred despite an increase in accumulation (Abdalati et al. 2004).

While there is general agreement between our varve record and regional glacier activity on decadal to centennial scales, weak correlations are found on shorter intervals (ex. using 5- and 9-year running averages). Although the varve thickness and accumulation rate time series likely contain additional paleoenvironmental information, previous studies from proglacial lakes show that varve thickness is often related in a very complex way to climatic variables (Lamoureux and Gilbert 2004; Tomkins and Lamoureux 2005; Menounos 2006; Hodder et al. 2007; Chutko and Lamoureux 2008). At the Lake Tuborg coring location, sedimentation is likely an integration of multiple interacting processes, including sediment flux from snowmelt, glacial melt, precipitation, and episodic slush flows; disentangling these influences on the varve record is beyond the scope of this article. The coring location was chosen to minimize the potential for unconformities and maximize the potential for recording and preserving jökulhlaup-derived sedimentation. By contrast, the cores analyzed by Smith et al. (2004) are much closer to the largest glacially-fed stream that enters Lake Tuborg (Fig. 1c, location iv), which likely explains why they found stronger links between varve thickness, Agassiz Ice Cap melt, and air temperature.

The highest correlation coefficients between the varve record presented here and previous records from the lake (Smith et al. 2004) generally occur for accumulation-rate time series that have not been adjusted by removing coarse beds and jökulhlaup deposits (Table 3). This is reasonable since these deposits were not removed from the Smith et al. (2004) time series. Correlation coefficients are surprisingly high given the likelihood of localized sedimentation controlled by multiple hydroclimatic, geomorphic and lacustrine processes (Hodder et al. 2007).

Chronology

The chronology from 2003 to 1963 is robust considering the correspondence between peak ^{137}Cs activity and laminae counting (Fig. 6). Field observations and remote-sensing imagery also show that the latest part of the chronology is accurate. The 1993 jökulhlaup was inferred from CTD casts in the lake and observation of kettle holes, raised shorelines, and a portal in 1995 (Phelps 1996; Lewis et al. 2007). Also, aerial photographs and field observations suggest a jökulhlaup occurred sometime between 1960 and 1963 (Hattersley-Smith and Serson 1964; Lewis et al. 2007). The chronology beyond 1960 is only based on varve counting. While the varve counting technique employed here minimizes the effects of localized and coring induced unconformities, it is possible that chronological errors are a source of residuals in correlations to local and regional climate and proxy records. If the ^{14}C date is accurate, then the record is much longer than suggested from varve counts, and recent jökulhlaup deposits are even more anomalous. However, we consider this unlikely. In arctic watersheds, terrestrial organic material, particularly wood, frequently resides on land for long periods of time before being transported to lakes, and ^{14}C dates from lake sediments are very often hundreds of years too old (Abbott and Stafford 1996; Child and Werner 1999; Zolitschka 1996; Wolfe et al. 2004; Oswald et al. 2005; Besonen et al. 2008).

Conclusions

A threshold was passed in 1960, when the ice-dammed lake above Lake Tuborg suddenly changed its drainage style from ice-dam overspilling to complete drainage by ice-dam flotation and tunnel development. Only three large jökulhlaups have occurred: 1960, 1993, and 2003. The change in drainage style was likely caused by thinning of the ice dam or deepening of the ice-dammed lake, which is consistent with long term and recent records of glacier ice-cap thinning and retreat in the region. Continued warming will likely increase expansion of the ice-dammed lake and its filling rate, and thin its dam, leading to increased jökulhlaup frequency and decreased magnitude. Another threshold may be reached when meltwater can no longer be stored in the ice-dammed lake, either because of retreat of the glacier dam, or thinning of the dam prevents resealing of the tunnel system (Clague and Evans 1994; Tweed and Russell 1999; Marren 2005). This threshold has not yet been reached, since the conduit system closed after the 2003 event, and the lake is currently refilling.

Acknowledgments This research was supported by National Science Foundation (NSF) grant ATM-9708071, ATM-0402421, ARC-0454959, NSF Doctoral Dissertation Research Improvement Award 0221376, Geological Society of America graduate student grants, an Arctic Institute of North America grant-in-aid, and the Gloria A. Radke prize from the University of Massachusetts. The Polar Continental Shelf Project (PCSP) and VECO Polar Resources provided outstanding logistical support. Mark Abbott, Whit Patridge, and Joe Stoner expertly retrieved the vibracores. Lesleigh Anderson, James Bradbury, David Mazzucchi, Joe Rogers, Anders Romundset, and Chloë Stuart also provided field assistance. Cores were photographed at the Limnological Research Center, Department of Geology and Geophysics, University of Minnesota-Twin Cities. John Brady kindly provided instruction and time on the Smith College Geology Department XRD. This is PCSP contribution number 03708.

References

Abbott MB, Stafford TW Jr (1996) Radiocarbon geochemistry of modern and ancient Arctic lake systems, Baffin Island, Canada. Quat Res 45:300–311. doi:10.1006/qres.1996.0031

Abdalati W, Krabill W, Frederick E, Manizade S, Martin C, Sonntag J et al (2004) Elevation changes of ice caps in the Canadian Arctic Archipelago. J Geophys Res. doi:10.1029/2003JF000045

Atwater BF (1984) Periodic floods from glacial Lake Missoula into the Sanpoil arm of glacial Lake Columbia, northeastern Washington. Geology 12:464–467. doi:10.1130/0091-7613(1984)12<464:PFFGLM>2.0.CO;2

Besonen M, Patridge W, Bradley RS, Francus P, Stoner JS, Abbott MB (2008) A record of climate over the last millennium based on varved lake sediments from the Canadian High Arctic. Holocene 18:169–180. doi:10.1177/0959683607085607

Best JL, Kostaschuk RA, Peakall J, Villard PV, Franklin M (2005) Whole flow field dynamics and velocity pulsing within natural sediment-laden underflows. Geology 33:765–768. doi:10.1130/G21516.1

Blais-Stevens A, Clague JJ, Mathewes RW, Hebda RJ, Bornhold BD (2003) Record of large, Late Pleistocene outburst floods preserved in Saanich Inlet sediments, Vancouver Island, Canada. Quat Sci Rev 22:2327–2334. doi:10.1016/S0277-3791(03)00212-9

Braun C (1997) Streamflow and sediment transport prediction in two High Arctic watersheds, Nunavut, Canada. Geosciences. University of Massachusetts, Amherst, p 167

Braun C, Hardy DR, Bradley RS (2000) Hydrological and meteorological observations at Lake Tuborg, Ellesmere Island, Nunavut, Canada. Polar Geogr 24:83–97

Child JK, Werner A (1999) Evidence for a hardwater radiocarbon dating effect, Wonder Lake, Denali National Park and Preserve, Alaska. Géogr Phys Quat 53:407–411

Chutko KJ, Lamoureux SF (2008) Identification of coherent links between interannual sedimentary structures and daily meteorological observations in Arctic proglacial lacustrine varves: potentials and limitations. Can J Earth Sci 45:1–13. doi:10.1139/E07-070

Clague JJ, Evans SG (1994) Formation and failure of natural dams in the Canadian Cordillera. Geological Survey of Canada Bulletin, Ottawa, ON, 35 pp

Fisher DA, Koerner RM, Reeh N (1995) Holocene climatic records from Agassiz Ice Cap, Ellesmere Island, NWT, Canada. Holocene 5:19–24. doi:10.1177/095968369500500103

Francus P (1998) An image analysis technique to measure grain-size variation in thin sections of soft clastic sediments. Sediment Geol 121:289–298. doi:10.1016/S0037-0738(98)00078-5

Francus P, Asikainen C (2001) Subsampling unconsolidated sediments: a solution for the preparation of undisturbed thin-sections from clay-rich sediments. J Paleolimnol 26:323–326

Francus P, Keimig F, Besonen M (2002) An algorithm to aid varve counting and measurement from thin-sections. J Paleolimnol 28:283–286. doi:10.1023/A:1021624415920

Gilbert R, Desloges JR, Clague JJ (1997) The glacilacustrine sedimentary environment of Bowser Lake in the northern Coast Mountains of British Columbia, Canada. J Paleolimnol 17:331–346

Gilbert R, Crookshanks S, Hodder KR, Spagnol J, Stull RB (2006) The record of an extreme flood in the sediments of montane Lillooet Lake, British Columbia: implications for paleoenvironmental assessment. J Paleolimnol 35:737–745. doi:10.1007/s10933-005-5152-8

Håkanson L, Jansson M (1983) Principles of lake sedimentology. Springer-Verlag, New York

Hattersley-Smith G, Serson H (1964) Stratified water of a glacial lake in northern Ellesmere Island. Arctic 17:108–111

Head KH (1992) Manual of soil laboratory testing. Pentech Press, London, 388 pp

Hodder KR, Gilbert R, Desloges JR (2007) Glaciolacustrine varved sediment as an alpine hydroclimatic proxy. J Paleolimnol 38:365–394. doi:10.1007/s10933-006-9083-9

Koerner RM (2005) Mass balance of glaciers in the Queen Elizabeth Islands, Nunavut, Canada. Ann Glaciol 42:417–423. doi:10.3189/172756405781813122

Lamoureux SF, Bollmann J (2004) Image acquisition. In: Francus P (ed) Image analysis, sediments and paleoenvironments. Springer, Dordrecht, pp 11–34

Lamoureux SF, Gilbert R (2004) A 750-year record of autumn snowfall and temperature variability and winter storminess recorded in the varved sediments of Bear Lake, Devon Island, Arctic Canada. Quat Res 61:134–147. doi:10.1016/j.yqres.2003.11.003

Lamoureux SF, England JH, Sharp MJ, Bush BG (2001) A varve record of increased 'little ice age' rainfall associated with volcanic activity, Arctic archipelago, Canada. Holocene 11:243–249. doi:10.1191/095968301668776315

Lewis T, Gilbert R, Lamoureux SF (2002) Spatial and temporal changes in sedimentary processes at proglacial Bear Lake, Devon Island, Nunavut. Arct Antarct Alp Res 34:119–129. doi:10.2307/1552463

Lewis T, Francus P, Bradley RS (2007) Limnology, sedimentology, and hydrology of a jökulhlaup into a meromictic high arctic lake. Can J Earth Sci 44:791–806. doi:10.1139/E06-125

Long A (1967) Age of trapped sea-water at the bottom of Lake Tuborg, Ellesmere Island, N.W.T. Trans Am Geophys Union 48:136

Maag H (1969) Ice-dammed lakes and marginal glacial drainage on Axel Heiberg Island, Axel Heiberg Island research reports. McGill University, Montreal, p 147

Maria A, Carey S, Sigurdsson H, Kincaid C, Helgadóttir G (2000) Source and dispersal of jökulhlaup sediments discharged to the sea following the 1996 Vatnajökull eruption. Geol Soc Am Bull 112:1507–1521. doi:10.1130/0016-7606(2000)112<1507:SADOJK>2.0.CO;2

Marren PM (2005) Magnitude and frequency in proglacial rivers: a geomorphological and sedimentological perspective. Earth Sci Rev 70:203–251. doi:10.1016/j.earscirev.2004.12.002

Menounos B (2006) Anomalous early 20th century sedimentation in proglacial Green Lake, British Columbia, Canada. Can J Earth Sci 43:671–678. doi:10.1139/E06-016

Ohlendorf C, Niessen F, Weissert H (1997) Glacial varve thickness and 127 years of instrumental climate data: a comparison. Clim Change 36:391–411. doi:10.1023/A:1005376913455

Old GD, Lawler DM, Snorrason Á (2005) Discharge and suspended sediment dynamics during two jökulhlaups in the Skaftá river, Iceland. Earth Surf Process Landf 30:1441–1460. doi:10.1002/esp. 1216

Oswald WW, Anderson PM, Brown TA, Brubaker LB, Hu FS, Lozhkin AV et al (2005) Effects of sample mass and macrofossil type on radiocarbon dating of arctic and boreal lake sediments. Holocene 15:758–767. doi:10.1191/0959683605hl849rr

Phelps KJ (1996) Laminated lacustrine sediments from glacial Lake Tuborg, Northern Ellesmere Island, Canada. Department of Geology, Bates College, Lewiston, p 85

Rittenour TM, Brigham-Grette J, Mann ME (2000) El Niño-like climate teleconnections in New England during the Late Pleistocene. Science 288:1039–1042. doi:10.1126/science.288.5468.1039

Rushmer EL, Russell A, Tweed FS Knudsen Ó, Marren PM (2002) The role of hydrograph shape in controlling glacier outburst flood (jökulhlaup) sedimentation. The structure, function and management implications of fluvial sedimentary systems. International Association of Hydrological Sciences, publication no. 276, Alice Springs, AU, pp 305–313

Schiefer E (2006) Depositional regimes and areal continuity of sedimentation in a montane lake basin, British Columbia, Canada. J Paleolimnol 35:617–628. doi:10.1007/s10933-005-5265-0

Scranton MI, Astor Y, Bohrer R, Ho T-Y, Muller-Karger F (2001) Controls on temporal variability of the geochemistry of the deep Cariaco Basin. Deep Sea Res Part I Oceanogr Res Pap 48:1605–1625. doi:10.1016/S0967-0637(00)00087-X

Smith ND, Ashley GM (1985) Proglacial lacustrine environment. In: Ashley GM, Shaw J, Smith ND (eds) Glacial sedimentary environments. Society of Paleontologists and Mineralogists, Tulsa, pp 135–246

Smith SV, Bradley RS, Abbott MB (2004) A 300 year record of environmental change from Lake Tuborg, Ellesmere Island, Nunavut, Canada. J Paleolimnol 32:137–148. doi:10.1023/B:JOPL.0000029431.23883.1c

Stewart KA, Lamoureux SF, Finney BP (2007) Multiple ecological and hydrological changes recorded in varved sediments from Sanagak Lake, Nunavut, Canada. J Paleolimnol. doi:10.1007/s10933-007-9153-7

Stuiver M, Reimer PJ (2005) Radiocarbon calibration program Calib. http://calib.qub.ac.uk/calib/. Last accessed July 16, 2008

Tomkins JD, Lamoureux SF (2005) Multiple hydroclimatic controls over recent sedimentation in proglacial Mirror Lake, southern Selwyn Mountains, Northwest Territories. Can J Earth Sci 42:1589–1599. doi:10.1139/e05-049

Trettin HP (1996) Geology, parts of Greely Fiord East, Greely Fiord West and Cañon Fiord, District of Franklin, Northwest Territories. Geological Survey of Canada, Map 1888A, scale 1:250 000

Tweed FS, Russell AJ (1999) Controls on the formation and sudden drainage of glacier-impounded lakes: implications for jökulhlaup characteristics. Prog Phys Geogr 23:79–110

Waitt RB (1984) Periodic jökulhlaups from Pleistocene glacial Lake Missoula—new evidence from varved sediment in northern Idaho and Washington. Quat Res 22:46–58. doi:10.1016/0033-5894(84)90005-X

Weirich FH (1986) The record of density-induced underflows in a glacial lake. Sedimentology 33:261–277. doi:10.1111/j.1365-3091.1986.tb00535.x

Wolfe AP, Miller GH, Olsen CA, Forman SL, Doran PT, Holmgren SU (2004) Geochronology of high latitude lake sediments. In: Pienitz R, Douglas MSV, Smol JP (eds) Long-term environmental change in Arctic and Antarctic Lakes. Springer, Dordrecht, pp 19–52

Zolitschka B (1996) Recent sedimentation in a high arctic lake, northern Ellesmere Island, Canada. J Paleolimnol 16:169–186. doi:10.1007/BF00176934

Zwally HJ, Schutz R, Bentley C, Bufton J, Herring T, Minster J et al (2003, updated 2007) GLAS/ICESat L2 Global land surface altimetry data, release 28. National Snow and Ice Data Center, Boulder, CO. Digital Media